Journal of
Mechanics of
Materials and Structures

BEHAVIOR OF PAPER ON A HIGH SPEED CONVEYOR SUBJECTED TO AIR JET IMPINGEMENT: A METHOD FOR ESTIMATING BENDING STIFFNESS

M. K. Ramasubramanian, Richard A. Venditti and Kalyan C. Katuri

Volume 2, Nº 2 February 2007

mathematical sciences publishers

JOURNAL OF MECHANICS OF MATERIALS AND STRUCTURES
Vol. 2, No. 2, 2007

BEHAVIOR OF PAPER ON A HIGH SPEED CONVEYOR SUBJECTED TO AIR JET IMPINGEMENT: A METHOD FOR ESTIMATING BENDING STIFFNESS

M. K. RAMASUBRAMANIAN, RICHARD A. VENDITTI AND KALYAN C. KATURI

Stiffness based sorting of mixed paper waste at high speed is desirable for sorting board, cardstock, and paper from each other for efficient recycling. We propose a quick, non-contact method for measuring the relative stiffness of paper samples moving on a conveyor at high speeds. The method consists of impinging an air jet on a moving paper sample while it is crossing a gap during transfer from one conveyor belt to another. The deflection caused by the impinging air jet can be measured and used to categorize different grades of paper. In this paper, we report results from a simulation of the proposed method using a finite element model. Influence of conveyor speed, sample orientation and nozzle pressure is studied using the model. Results indicate that the stiffness estimation has sufficient resolution to distinguish between board and paper grades at high conveyor speeds.

1. Introduction

The paper recycling industry is important world-wide, providing both economic and environmental benefits. Paper recycling significantly decreases landfill utilization rates and avoids landfilling costs and in many cases reduces the energy requirements to produce papermaking fibers relative to pulping wood. According to the AFPA Recovered Paper Statistical Highlights (2005 edition), in the year 2004 approximately 50 million tons of paper were recycled out of the 102 million tons available in the United States. This is a 49.5% recovery rate. Paper recycling thereby increases the efficient usage of natural resources. Optimized paper recycling requires a homogenous recovered paper feed stream [Pryor 2000]. Often, co-mingled paper is recovered as a convenient method to encourage higher recovery rates of paper despite this. The co-mingled paper of different grades can be sorted either manually or through automatic sorting processes [Arzoumanian 2000] so as to improve the subsequent economics of paper recycling. The quality of the recycled paper depends greatly on the effectiveness of the sorting procedure.

Typically, paper products are recycled into the same type of products. For instance recovered newspapers are recycled into newsprint, corrugated boxes are recycled into new boxes, sorted office waste is recycled into printing and writing grades. The reason is that each of these grades utilizes fibers of different chemistry and quality. Newsprint paper utilizes fibers that are short and essentially have the same composition as wood. These inexpensive fibers have high contents of lignin which cause the paper to yellow over time. Corrugated containers use longer fibers that have been chemically pulped. Products like copy paper must use highly bleached, high brightness fibers. Comingled waste has low value and can

Keywords: paper recycling, bending stiffness, paper sorting, copy paper, finite element model, cardboard.
Research supported by the U.S. Department of Energy under the Industries for the Future Program, Forest Products Industry Agenda 2020; project number DE-FC07-00ID13880.

only be utilized for the most inexpensive products with low quality demand such as tube stock or as board. The implementation of improved and more economical sorting processes will allow the conversion of co-mingled waste to homogenous streams that can be diverted to the most appropriate target product recycling process.

Sorting can also potentially be used to distinguish and separate common types of papers that need to have special consideration when recycled. These could include coated papers for publication, colored papers, wax coated papers and many other types. Currently sensors are available for sorting glossy paper, office paper, newsprint, and colored paper from the input feed. The glossy paper is sensed by using a sensor which measures the intensity of the glare from the surface of the paper sample. Colored paper can be identified by using a high speed camera or matrices of discrete color sensors. A lignin sensor which can distinguish between office paper and newsprint was described in [Ramasubramanian et al. 2005; Mallapragada et al. 2004; Nilsson et al. 2001; Roman and Jeffers 1992]. Large amounts of lignin, a fluorescing chemical compound, is present in newsprint fibers and not in copy paper fibers. The lignin sensor measures the amount of fluorescent radiation from the sample by first exciting the sample using a laser source and measuring the fluorescence intensity using a photo multiplier detection system.

The efficiency of the sorting procedure will be maximum when all the above mentioned sensors along with stiffness sensor work to provide input data to a central decision making algorithm residing in a micro-controller. The decision making algorithm can then be used for sample identification and for the actuation of the mechanisms to move the paper to different collection bins based on paper mill requirements [Singhal et al. 2001].

1.1. ***Stiffness sensing techniques.*** There has been a lot of development in the field of on-machine paper stiffness sensing. Most of the developed techniques are meant for testing paper webs in the paper manufacturing industry. The goal is to determine paper strength properties since they directly influence the quality of the paper and process parameters. The elastic stiffness properties of paper correlates well with paper strength properties. The stiffness properties of paper can be found by studying the dispersion curves of Lamb waves. Lamb waves are surface waves in plates. Dispersion characteristics of lamb wave modes in machine made paper were discussed by [Habeger et al. 1979] . Air coupled transducers can be used to generate Lamb waves on paper surface. However these transducers are not well suited for on-line implementation due to air turbulence at the surface of the fast-moving web. The paper thickness should also be high to excite lamb waves using these transducers [Habeger et al. 1979]. When a laser pulse is focused on the top surface of the paper, a transient displacement field results due to localized thermal expansion.Thermoelastic excitation of Lamb waves along the principal directions in machine made paper has been discussed in [Cheng and Berthelot 1996; Brodeur et al. 1997; Johnson 1996]. Ridgway et al. [1999] have compared the performance of three different interferometry techniques in measuring laser generated elastic wave phase velocities on paper moving at production speeds. Slight discrepancies were found in the non-contact measurements due to humidity variations. The ultrasonic wave velocities were also found to be very sensitive to water content and temperature of the paper. Walter et al. [2000] have used a Fabry–Perot detector and a tracking mirror to increase the optical efficiency of the detection system. This setup has avoided the ablation of paper material by not using a high intensity laser to generate elastic waves on paper surface. The determination of bending stiffness of paper using laser ultrasonics was demonstrated in [Cornwell et al. 2001]. A pulsed laser was used to excite lamb

waves and fiber optic Mach–Zehnder interferometer was used to detect the normal component of lamb waves. The dispersion curve obtained from the wavelet transform of the signal was compared to the material dispersion curve calculated using the material constants and both the curves were found to be in good agreement. Ridgway et al. [2003] estimated the flexural rigidity of paper web running at 5000 ft/min by measuring the frequency dependence of the phase velocity of A_0 mode lamb waves. While this method worked for fine paper grades, the low frequency signal amplitude from paperboard was found to be insufficient for making accurate measurements.

All the above mentioned techniques are meant to be used for testing the strength properties of paper webs of almost constant thickness values, that is, the thickness of the samples does not change drastically between two consecutive measurements. This is not the case in paper sorting. Unlike paper webs, the thickness of paper on a sorting conveyor varies widely from one sample to another. One sample might have high thickness like cardboard and the next one can be a finer grade paper such as copy paper. Therefore, the transducer input energy needs to be varied depending on the sample for getting better signal to noise ratio for each sample, which is difficult to achieve. In order to sort recovered paper, there is no need to find the exact elastic constants of each and every sample. The relative stiffness values should be sufficient to sort the paper into different bins and hence eliminates the need for complex and expensive equipment.

1.2. ***Proposed method.*** The relative bending stiffness sensor setup is shown in Figure 1. The idea is to apply a constant pneumatic pressure load on top of the paper sample spanning two supports that are a known distance apart. The two supports are two belt conveyors which are positioned one after another with a small clearance between them. The deflection of the sample to the load is inversely proportional to the stiffness of the sample. A distance sensor can be used to measure the deflection of paper due air jet impingement. Any of the distance sensing techniques such as optical, ultrasonic or RF could be used for measuring the paper deflection. The proposed method will be useful in distinguishing the samples based on their relative bending stiffnesses. While a static load-deflection curve can be generated and modeled using elementary mechanics, studying the method under dynamic conditions is the focus of this study.

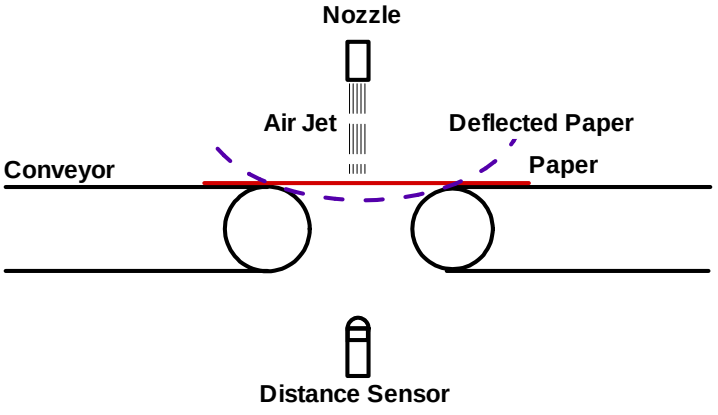

Figure 1. Bending stiffness sensing setup.

2. Finite element model

A finite element model of the paper-conveyor system was built to provide a detailed understanding of the sensor concept. A parametric study using the finite element model was carried out to provide a clear insight into the process parameters and their influence on the deflection of the sample. A macroscopic modeling approach was adopted for modeling the paper. This presupposes a homogeneous deformation field and does not account for local phenomenon [Ramasubramanian and Muthuraman 2003]. The model was built in ABAQUS/Explicit environment which is suitable for transient dynamic analysis problems such as this one. Direct-integration dynamic analysis procedure was used for finding the deflection of paper samples over the conveyor gap for various conveyor speeds and air jet loadings as it is computationally efficient for the analysis of large models with relatively short dynamic response times [ABAQUS 2003]. It is also suitable for the analysis of discontinuous events such as the current model, which contains several contact interactions that change rapidly during the analysis [Sun et al. 2000; Zhong 1993; Hughes 1987].

2.1. ***Model geometry.*** The paper-conveyor system was modeled in 3D space. The high speed conveyor is modeled using analytical rigid elements. Rectangular shaped analytical rigid surface is used for modeling the conveyor belt surface. The conveyor roller surfaces are modeled separately from the conveyor belt surface by using cylindrical analytical rigid surfaces. This discretization of the conveyor surface allows the specification of separate boundary conditions for flat and cylindrical surfaces of the belt conveyor. A clearance of 40 mm is specified between the roller surfaces of the two conveyors. The flat conveyor surface is constrained in all directions where as an angular velocity boundary condition is specified for both the conveyor rollers. This boundary condition simulates the rotating roller surface of the actual conveyor. The angular velocity of the rollers is computed from the speed of the conveyor. For a given value of conveyor speed, the angular velocity of the conveyor is found from the expression $\omega = V/R$, where ω is the angular velocity of the roller, V is the tangential velocity of the conveyor belt and $R = 4''$ is the roller radius. Paper is modeled as a thin rectangular plate sitting flat on the right conveyor belt

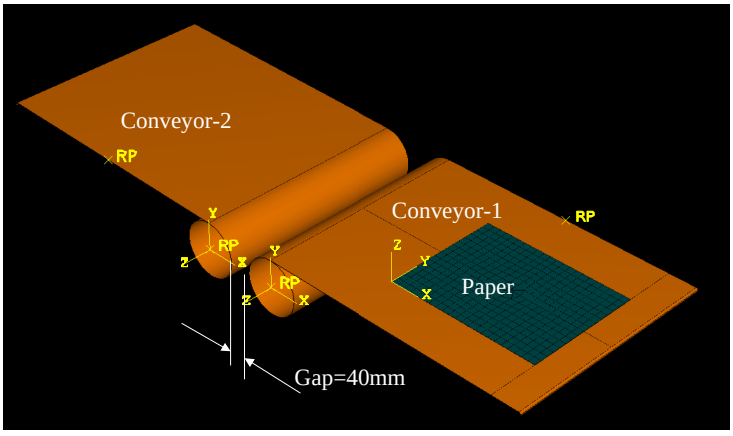

Figure 2. Assembled view of the model.

surface in the 1-3 plane. The assembled model consisting of paper and conveyor surfaces is shown in Figure 2.

To simulate the high-speed moving conveyor, a uniform initial velocity field is specified on the nodes of the paper sample. The magnitude of the velocity is specified to be equal to the tangential velocity of the conveyor belt. But in the real paper-conveyor system, the paper sample moves along with the conveyor belt and there will not be any relative motion between the two until the paper reaches the end of the conveyor. To meet this requirement, the interaction between the flat conveyor surface and the paper surface is modeled as frictionless.

2.2. ***Contact model.*** The contact behavior between the paper and the conveyor surfaces is modeled by specifying contact interactions between the surfaces that might come into contact during the course of the analysis. The Contact modeling involved two steps. In the first step, various surfaces that might come into contact during the analysis procedure are identified. Then these surfaces are coupled together by specifying them as contact pairs. In the second step, mechanical property models are assigned to the contact pairs. The contact property model specifies the normal and tangential behavior of the surfaces when they come into contact. The normal behavior between the paper surface and the conveyor surface is specified as hard. The "Hard" contact relationship minimizes the penetration of the paper element nodes into the conveyor surface and does not allow transfer of tensile stress across the interface. When the surfaces are in contact, any contact pressure can be transmitted between them. The surfaces separate if the contact pressure reduces to zero. Separated surfaces come into contact when the clearance between them reduces to zero. Kinematic predictor/corrector contact algorithm is used to enforce contact constraints. Finite sliding approach which allows arbitrary motion of the surfaces forming the contact pair is used for specifying the sliding between any two contact surfaces in the model.

Classical isotropic Coulomb friction model is used to specify the tangential behavior of the contacting surfaces. The standard Coulomb friction model assumes that no relative motion occurs if the equivalent frictional stress is less than the critical stress, $\tau_{critical}$ which is proportional to the contact pressure, p, in the form $\tau_{critical} = \mu p$, where μ is the friction coefficient that is defined as a function of the contact pressure p. The tangential behavior of the surface is defined by specifying the coefficient of friction between the contacting surfaces. For determining the coefficients of friction between the paper samples and the conveyor, the surface roughness of the conveyor and the paper needs to be known. The surface properties of the paper samples vary widely during the sorting procedure and it is hard to obtain the coefficients of friction for all possible surface combinations. Therefore, simplifying assumptions were made by considering the friction to be isotropic and to be independent of the contact pressure and other field variables. The surface roughness of the paper surface is less than the surface roughness of the conveyor roller. The coefficient of friction of driving pulley of steel for industrial conveyor is found to be equal to 0.15 from the specifications of the conveyor. The static coefficient of friction between the conveyor and the paper surface is assumed to be equal to half of that, 0.07, and the kinetic friction coefficient was set to be equal to 0.04. These friction coefficients are not the exact values. The actual values can only be found by first choosing the conveyor and measuring the friction coefficient for the conveyor and different paper grades that might be found in the input feed. The effective friction coefficient between the contacting surfaces is assumed to satisfy the equation described by [Oden and Martins 1985]:

$$\mu = \mu_k + (\mu_s - \mu_k)e^{-d_c \dot{\gamma}_{eq}}, \tag{1}$$

where μ_k is the kinetic coefficient of friction, μ_s is the static coefficient of friction, d_c is the decay coefficient and $\dot{\gamma}_{eq} = (\dot{\gamma}_1^2 + \dot{\gamma}_2^2)^{-1/2}$ is the slip rate with $\dot{\gamma}_i$ is the slip rate in the direction i. The decay coefficient specifies the rate at which the effective friction coefficient value reaches the value of kinetic coefficient of friction once the slip starts to occur. Totally four surfaces are identified in the Paper-conveyor model that can come into contact with the paper sample during the analysis, see Figure 3.

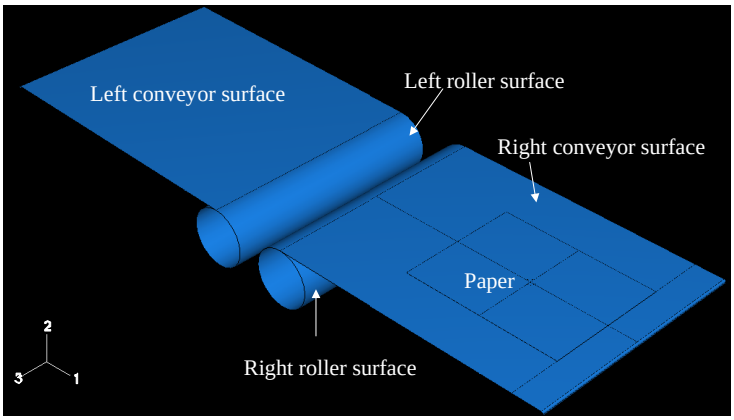

Figure 3. Potential contact surfaces for the paper sample.

Two mechanical contact interaction properties were created. The first property has hard normal behavior and frictionless tangential behavior. For the second property, the tangential behavior is specified to follow Equation (1). Four contact pairs are created and the interaction properties are assigned, see Table 1.

The tangential behavior between the paper surface and the conveyor surface is modeled as frictionless because there is no relative motion between the paper and the conveyor surface. Both of them will be moving at the same speed. There will be some slip between the paper surface and the left conveyor surface because the velocity of the paper will be reduced due to the applied pneumatic load. But that slip is neglected because its effect on the paper deflection is insignificant.

Contact Pair	**Interaction Property**	
	Tangential Behavior	Normal Behavior
Paper-Right conveyor surface	Frictionless	Hard
Paper-Right roller surface	Friction specified	Hard
Paper-Left roller surface	Friction specified	Hard
Paper-Left conveyor surface	Frictionless	Hard

Table 1. Contact interactions.

2.3. ***Material model.*** Even though paper is highly anisotropic at the microscopic level, it is treated as orthotropic at the macroscopic level [Makela and Ostlund 2003; Leppänen et al. 2005]. During the paper manufacturing process, most of the fibers are oriented in a direction parallel to the length of the paper web which is the Machine Direction (MD). The Cross Direction is perpendicular to the MD. The MD and CD of the paper are the in-plane principal material directions of the paper. The Young's modulus in MD is significantly higher than that of CD because of preferential alignment of the fibers. The constitutive relation for paper is

$$\begin{bmatrix} \varepsilon_{11} \\ \varepsilon_{22} \\ \varepsilon_{33} \\ \gamma_{12} \\ \gamma_{13} \\ \gamma_{23} \end{bmatrix} = \begin{bmatrix} 1/E_{MD} & -\nu_{21}/E_{CD} & -\nu_{31}/E_{ZD} & 0 & 0 & 0 \\ -\nu_{12}/E_{MD} & 1/E_{CD} & -\nu_{32}/E_{ZD} & 0 & 0 & 0 \\ -\nu_{13}/E_{MD} & -\nu_{23}/E_{CD} & 1/E_{ZD} & 0 & 0 & 0 \\ 0 & 0 & 0 & 1/G_{12} & 0 & 0 \\ 0 & 0 & 0 & 0 & 1/G_{13} & 0 \\ 0 & 0 & 0 & 0 & 0 & 1/G_{23} \end{bmatrix} \begin{bmatrix} \sigma_{11} \\ \sigma_{22} \\ \sigma_{33} \\ \sigma_{12} \\ \sigma_{13} \\ \sigma_{23} \end{bmatrix},$$

where the subscripts 1, 2 indicate machine and cross-machine directions. E_{MD}, E_{CD} and E_{ZD} are the Young's moduli in the machine, cross-machine and thickness directions. respectively. G_{12} is the in-plane shear modulus and G_{13}, G_{23} are the out-of-plane shear moduli.

The properties of the paper samples are obtained by mechanical testing. Three grades of paper that are commonly found in the recovered paper were tested using the Minimat tensile tester (Rheometrics, Inc). Thin strips of paper of size 1 cm $\times$ 5 cm were cut both in machine and cross machine directions and tested to get the Young's moduli. Flat faced screw clamps were used to hold the paper strips. The tests were conducted in a non-conditioned environment at a cross-head speed of 1 inch/min. The thicknesses of paper grades were measured with a hard platen. Engineering estimates were made for the Poisson's ratio and the out of plane shear moduli of the three paper grades based on the results obtained by [Mann et al. 1980]. Since the effect of transverse shear deformation is negligible for very thin samples such as paper, the out of plane shear moduli is assumed to be same for all the three grades. An optimization technique as discussed by [Seo et al. 1992] was used for finding the in plane shear modulus. The goal of this method is to perform the measurements of the Young's moduli in the optimum angular region (the so-called error boundary) to achieve the best accuracy in the determination of G_{12}. According to this method, the anisotropy of the Young's moduli was found by finding the ratio of E_{MD} to E_{CD} and it was used for finding the minimum error boundary region. The stress-strain curves were obtained at an angle θ (minimum error angle), $\theta - 5^\circ$ and $\theta + 5^\circ$ in addition to machine and cross-machine directions; see Figure 4. A least-squares algorithm was used to estimate the shear modulus best fitted to the experimental data: see Table 2.

Since the lateral (in-plane) dimensions of the paper are much larger than the thickness of the paper, plane stress shell elements are used for modeling the paper surface. These elements also allow transverse shear deformation. Kirchoff's thin shell theory is used for the 3D paper model, implying that a material line that is originally normal to the mid-surface of the shell elements remains so throughout the deformation. Transverse shear stress acts as penalty function to impose Kirchoff's constraints. The shell elements also account for finite membrane strains and arbitrarily large rotations. Each element has four nodes at which element variables are calculated and use linear interpolation in each direction to find the displacements at any other point in the element. Each node has six degrees of freedom which include

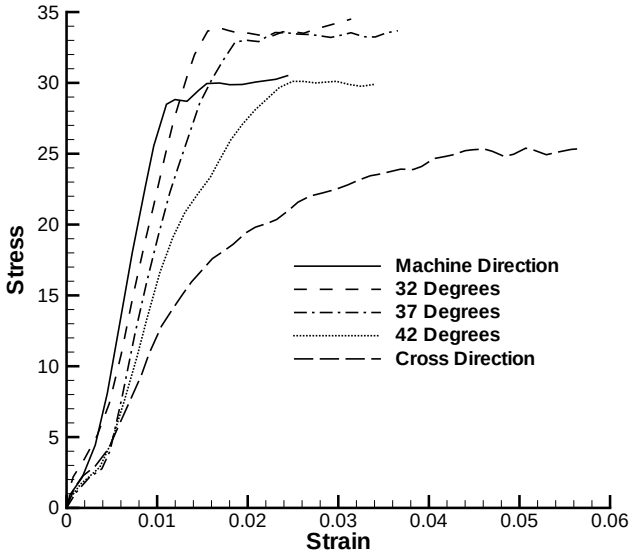

Figure 4. Light-weight paper stress strain curves in different directions relative to the machine direction.

both the rotational and translational degrees of freedom. Even though the shell elements allow transverse shear deformation, it becomes very small as the shell thickness decreases. Therefore, the error due to the estimated out of plane shear moduli is negligible. The in-plane dimensions of the paper sample are specified to be equal to the standard letter paper size: $11'' \times 8.5''$. The machine direction of the paper is specified to be parallel to the length of the paper and cross-machine direction is specified to be parallel to the width of the paper.

2.4. ***Loading conditions.*** The external loads acting on the paper sample are: the load due to surrounding air, weight of the paper and the pneumatic load that acts on the paper when it passes over the gap. The

	Light-weight paper	**Medium card stock**	**Heavy card stock**	**Method**
Thickness, μm	105	206	229	Measured
Basis weight, g/m^2	75	145	200	Measured
E_{MD}, GPa	3.98	1.69	1.79	Measured
E_{CD}, GPa	1.27	1.11	1.09	Measured
ν_{12}	0.15	0.15	0.15	Estimated
G_{12}, GPa	0.93	0.71	0.63	Computed
G_{13}, GPa	0.35	0.35	0.35	Estimated
G_{23}, GPa	0.35	0.35	0.35	Estimated

Table 2. Input parameters.

load due to the air surrounding the paper sample is modeled as a viscous pressure load whose magnitude is equal to the atmospheric pressure; see Figure 5.

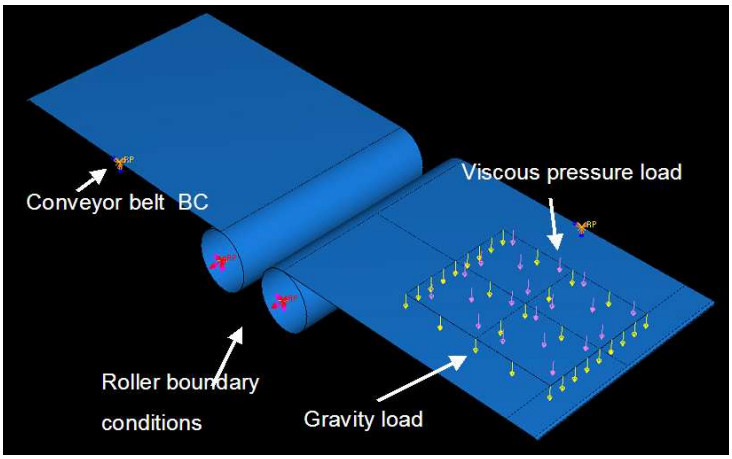

Figure 5. Specified loading and boundary conditions.

The pneumatic load due to the nozzle does not act continuously on the paper sample but acts when the sample jumps over the clearance between the two conveyors. To simulate this loading behavior, a set of elements was created by specifying circular partition on the top surface of the paper and the time history of the load on the element set was prescribed by using the amplitude curves. The amplitude curve specifies the load on a set of elements as a function of time. By initially positioning the paper sample at a known distance from the center of the gap, the position of the paper sample as a function of the analysis

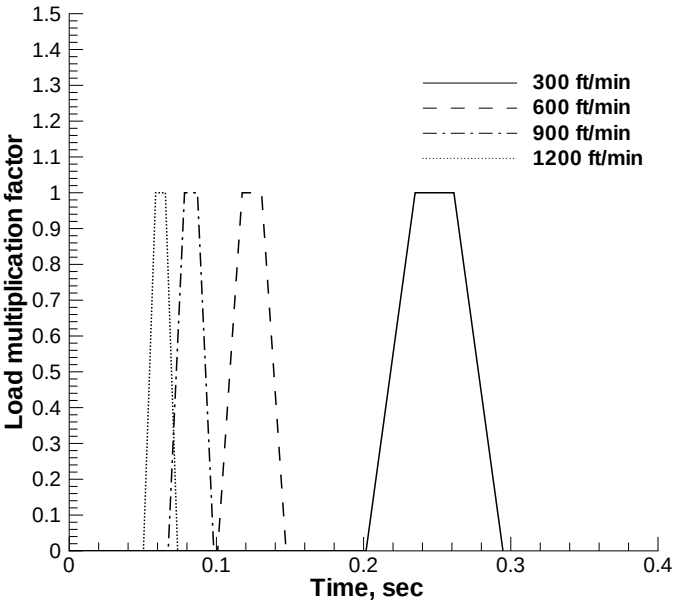

Figure 6. Amplitude curves for different conveyor speeds.

Nozzle inlet pressure, psi	Load intensity N/m^2
10	1293.91
20	2391.52
25	3952.28
30	4641.43
Nozzle height $= 1''$	
Spread area = $76 \pm 0.73\,mm^2$	

Table 3. Cylindrical spread nozzle data.

time can be roughly known from the initial velocity of the paper sample. This information was used to construct the amplitude curves for different conveyor speeds; see Figure 6.

At any time during the analysis, the actual load applied on the element set will be equal to the product of the maximum load value given on the input data line and the load multiplication factor at that instant of time, which was obtained from the amplitude curve. In this way, the paper samples will be loaded only when they reach the gap between the two conveyors. To obtain the load intensity and spread area data, several nozzles with different profiles were investigated to find effective nozzle for the sorting procedure. A cylindrical stream nozzle (Series 544 with orifice diameter $d = 0.032$ inches from Lechler, Inc.) which produces a concentrated direct stream of air was selected and the load distribution data of

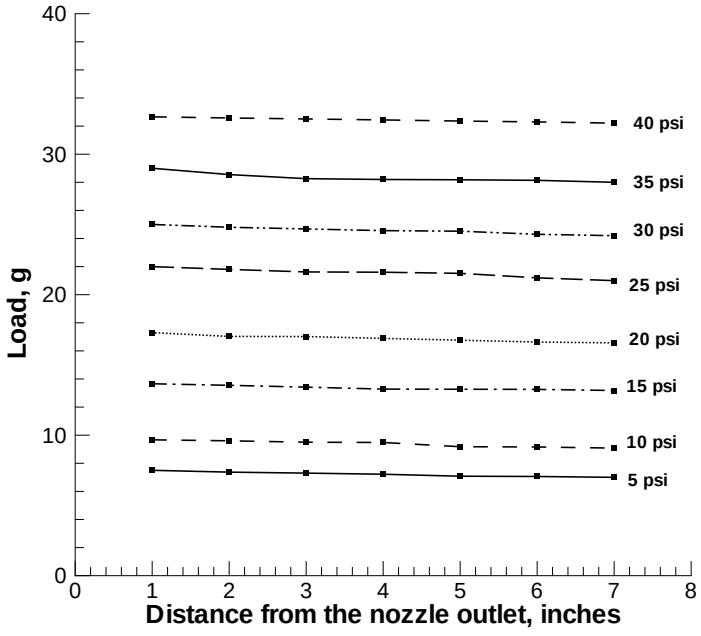

Figure 7. Cylindrical nozzle load profile.

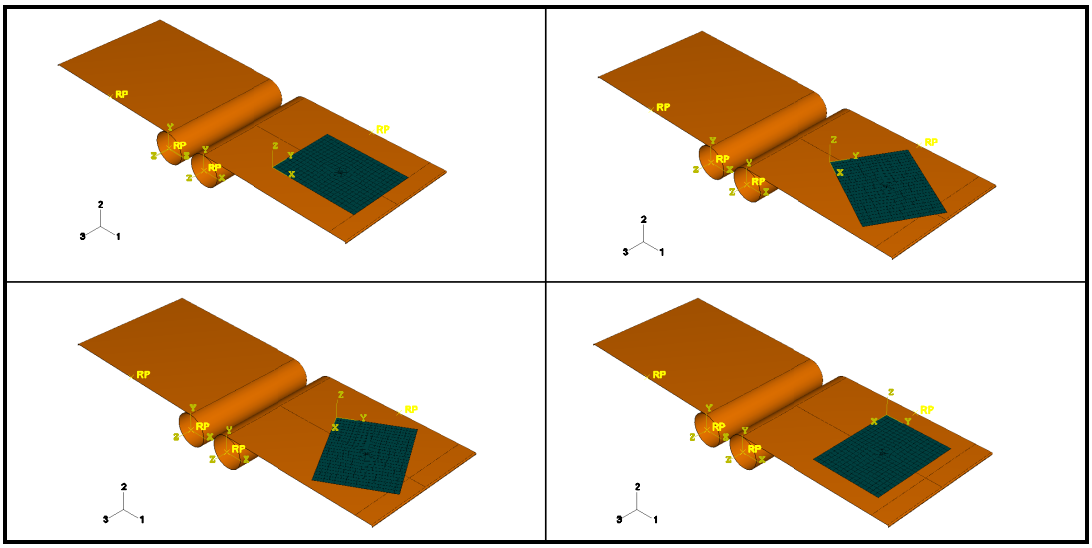

Figure 8. Paper sample with its machine direction oriented at 0°, 30°, 60°, 90° to the conveyor travel direction.

the nozzle was obtained experimentally. This data was used for specifying the circular partition diameter and the maximum load intensity on the elements in the set, see Table 3 and Figure 7.

2.5. ***Simulation.*** The deflection values were obtained for three paper grades as a function of load, conveyor speed and the orientation of the samples on the conveyor belt. Deflection values of the samples were found at four nozzle loads. All the nozzle loads used in the simulation were obtained from the load intensity data of the cylindrical profile nozzle when it was operating at different inlet pressures and held at a distance of one inch above the conveyor surface. The samples were loaded when the machine direction was oriented parallel to conveyor travel direction, and when machine direction was at 30°, 60°, 90° to the conveyor travel direction; see Figure 8. The deflection behavior of the paper for all the four loading conditions was observed at the conveyor speeds of 300 ft/min and 1200 ft/min.

The deflection values are measured relative to the flat conveyor surface. The deflections are considered positive when the paper rises above the flat conveyor surface and negative when the paper deflects downwards below the conveyor surface due to the applied load. This happens when the paper spans the gap between the two conveyors.

3. Results

In order to identify the effects of atmospheric pressure on the paper sample, a finite element model was created with all the loading and boundary conditions as mentioned earlier except for the atmospheric pressure and the external pneumatic load. Figure 9 shows the results: (1) shows the state of the paper at the start of the simulation; (2) shows the state of the paper after it has crossed the gap and has touched the second conveyor surface; (3), (4) and (5) show the sheet leaving the surface of the conveyor due to lack of damping force; (6) shows the sheet moving downwards due to gravity. In the next simulation the ambient air pressure was specified on the top surface of the paper sample. All the remaining boundary

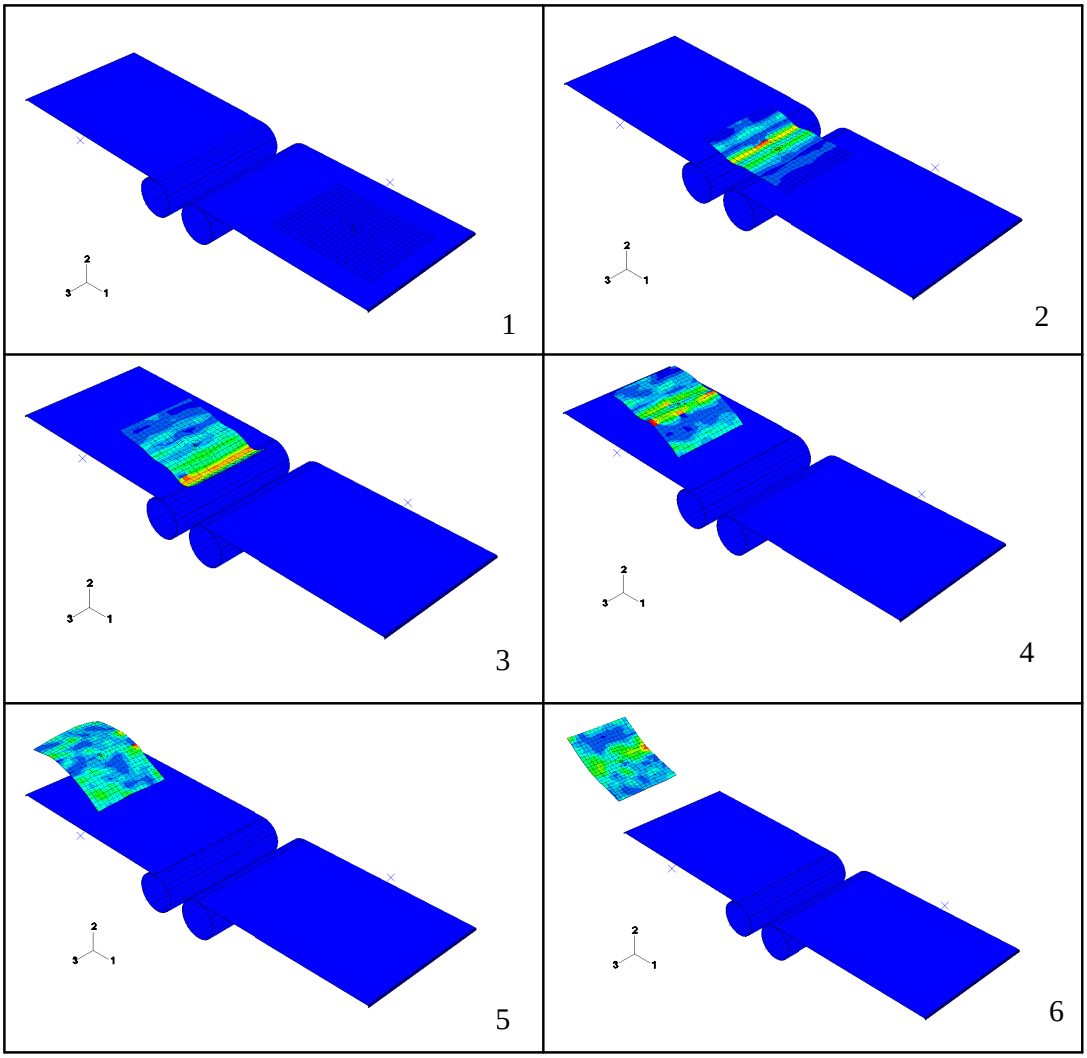

Figure 9. Response of the paper sample moving at 300 ft/min in the absence of viscous pressure.

and loading conditions were kept the same as the earlier simulation. In this case (Figure 10), the paper does not leave the conveyor surface as in the earlier case; the pressure keeps the sheet on the conveyor after crossing over. This indicates the importance of the air pressure acting as a damping medium on the paper surface.

Next, two sets of simulations were run by specifying two different conveyor speeds. For each speed, the sample deflections are found at each of the four nozzle inlet pressures and at different orientations of the paper on the conveyor. The deflection of the paper due to applied pneumatic load is found by measuring the maximum displacement of the center node of the circular partitioned element set in the downward direction. For the first set of simulations, the conveyor speed is set to be equal to 300 ft/min and deflections were measured for the three paper grades due to the pneumatic loads acting at the nozzle

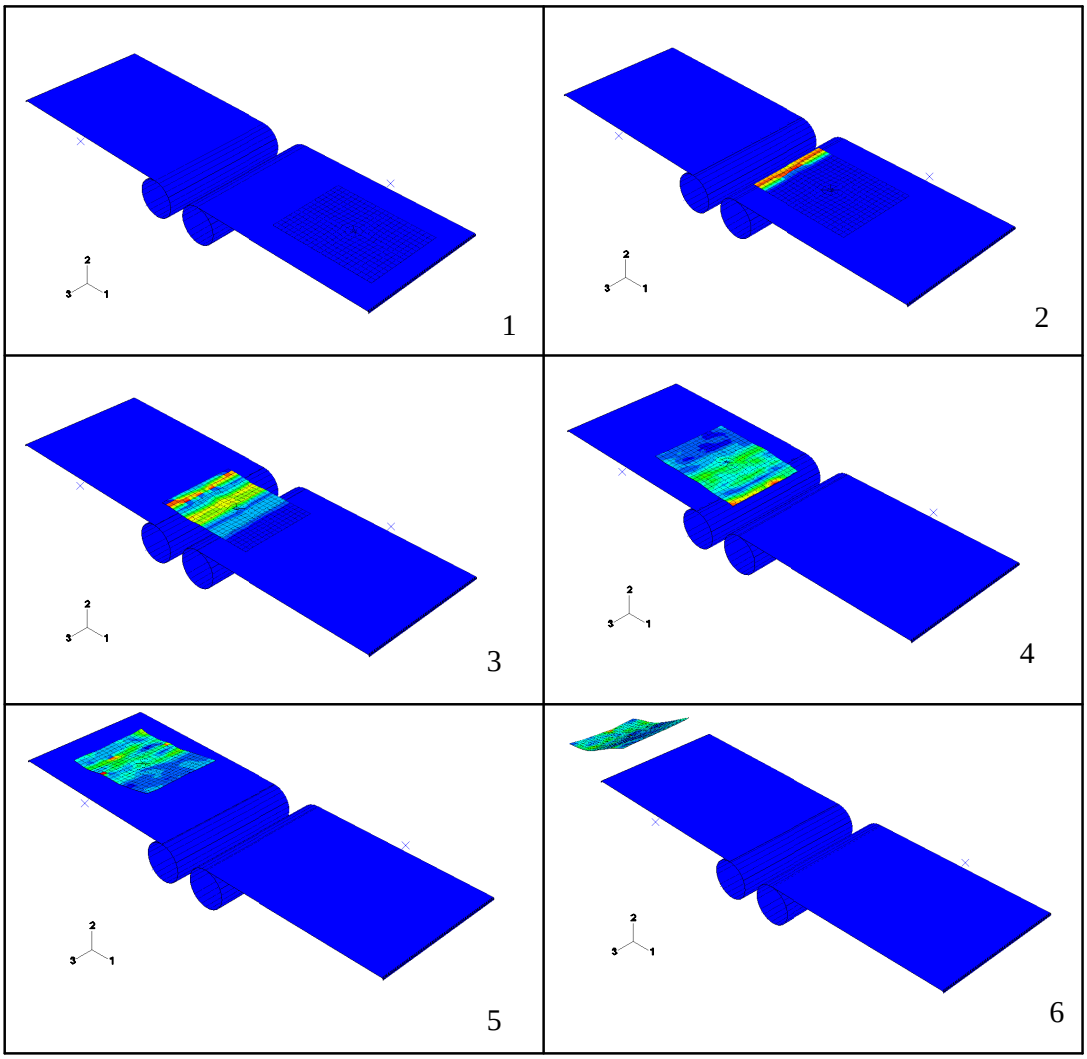

Figure 10. Response of the paper sample moving at 300 ft/min in the presence of viscous pressure.

inlet pressures of 10, 20, 25 and 30 psi, respectively. The light-weight paper was able to clear the gap only when its MD was less than 30° to the conveyor length direction and the nozzle input pressure was 10 psi. In all other cases, it was unable to clear the gap; see Figure 11, which shows paper deflection values for samples that were able to withstand the pneumatic load. The heavy card stock had no difficulty in clearing the gap when the load was applied, as was expected since its flexural rigidity is higher than that of the light-weight paper. The response of the light-weight paper and the heavy card stock when they were loaded in CD is shown in Figure 12. The medium card stock also failed to clear the gap at the nozzle inlet pressure of 30 psi; see Figure 11, right. The deflection values increase as the orientation of the paper changes from MD to CD.

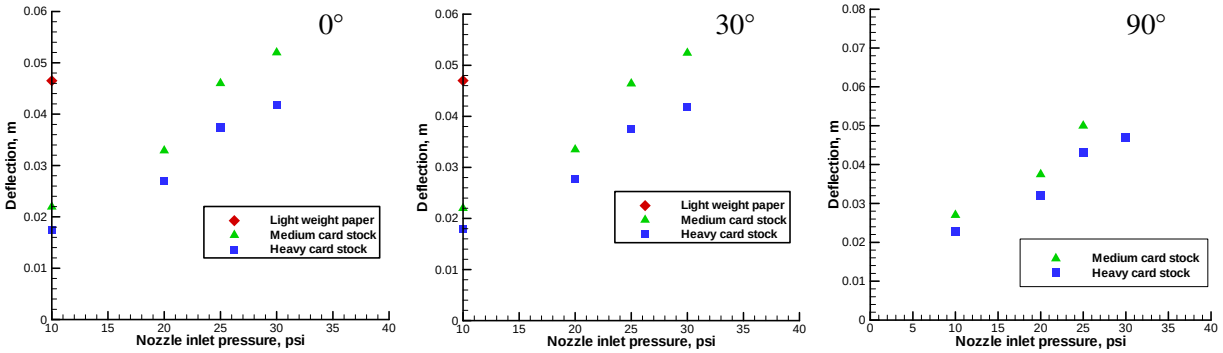

Figure 11. Deflection of the paper samples moving at 300 ft/min. Angles indicate paper orientation (see Figure 8 for convention).

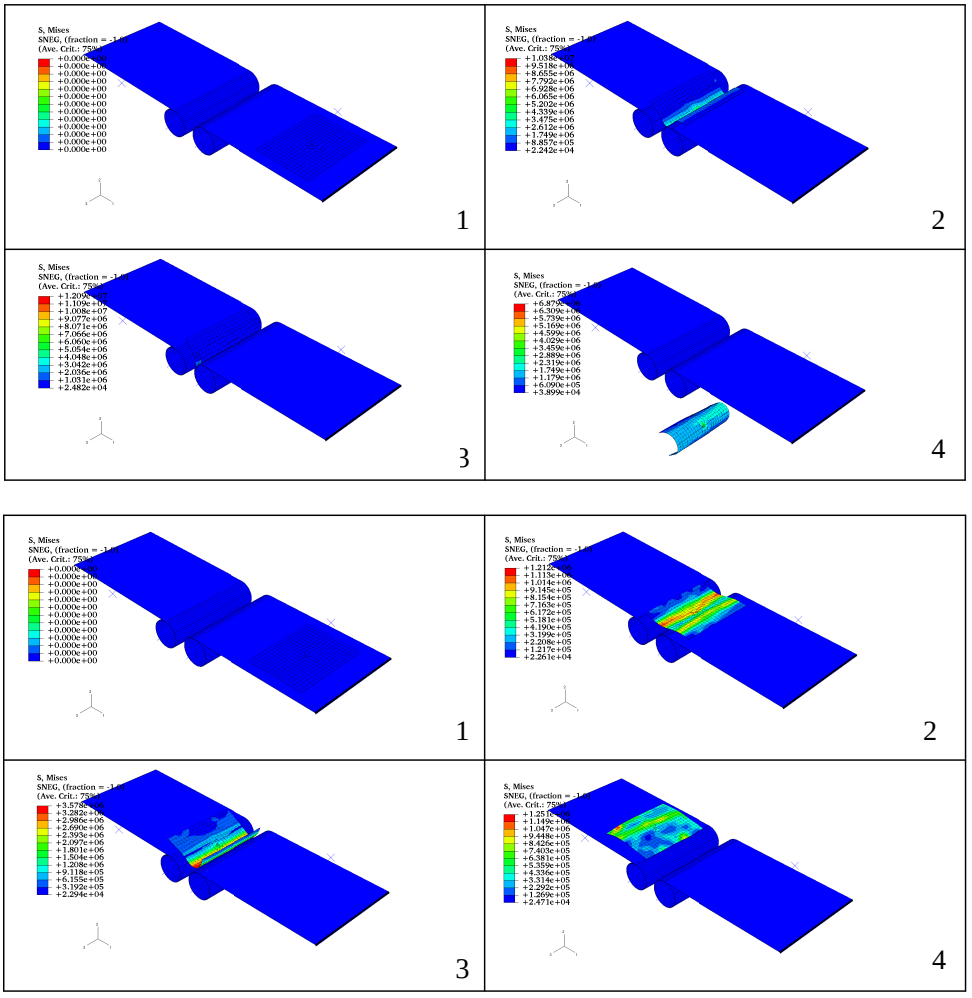

Figure 12. Response of paper loaded in CD and moving at 300 ft/min. Top four panes: light-weight paper; bottom: heavy card stock.

During the second set of the simulations, the speed of the conveyor was increased from 300 ft/min to the expected operating speed of 1200 ft/min. The loading and boundary conditions were kept the same. In this case all paper samples cleared the gap for all four nozzle; see Figure 13.

The deflection, however, decreased significantly compared to that of the samples moving at 300 ft/min. This is expected because the samples moving at 1200 ft/min are subjected to air jet load for a shorter amount of time than the samples moving at 300 ft/min. The deflections increased as the orientation of the machine direction of the paper sample increase from 0° to 90° with respect to the conveyor travel direction. This is because of the lower values of the Young's modulus of the sample in cross-machine direction when compared to the machine direction.

After the paper moves past the gap, the paper does not immediately land completely on the other conveyor surface because of the disturbance caused by the momentary application of the pneumatic load. This is illustrated in the Figure 14. The heavy card stock does not closely follow the conveyor surface at 1200 ft/min when compared to 300 ft/min.

Another important aspect is the settling time which the samples take to settle completely on the left conveyor surface after clearing the gap. The samples moving at 300 ft/min took less time to settle on the conveyor surface than those moving at 1200 ft/min. The time histories of the three paper grades during the analysis at the two conveyor speeds are shown in Figure 15. It is evident from the response curves that the paper samples exhibit more positive displacement at 1200 ft/min as compared to 300 ft/min.

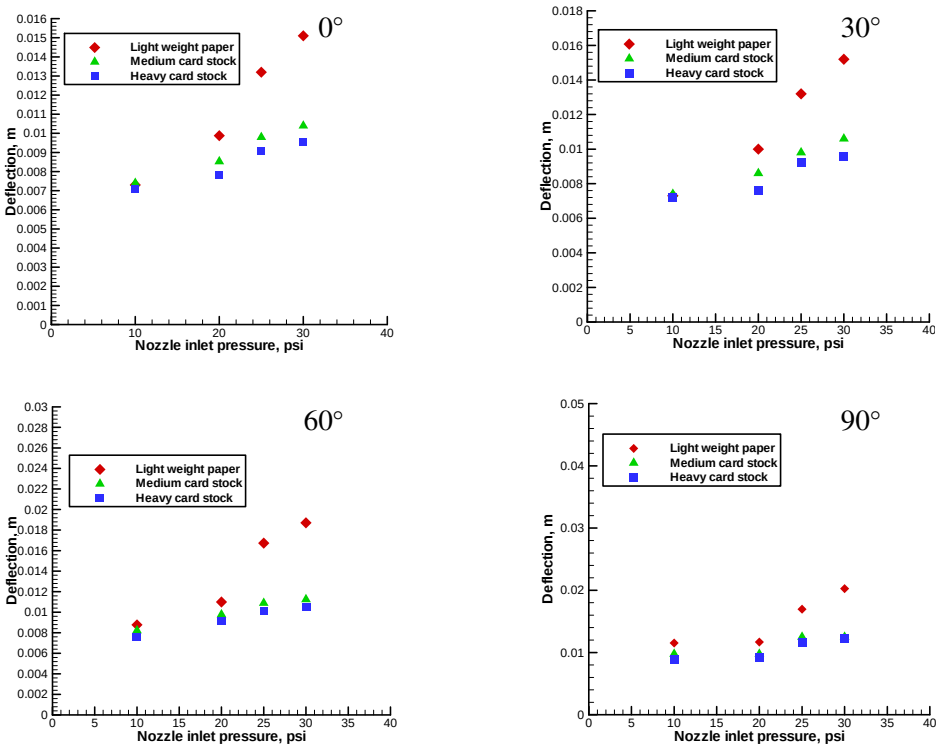

Figure 13. Deflection of the paper samples moving at 1200 ft/min. Angles indicate paper orientation.

The light-weight paper has higher negative deflection values since it failed to withstand the load when moving at 300 ft/min; see Figure 15.

The bending stiffnesses and deflections of the three paper grades in the machine direction were computed and normalized with respect to the corresponding values of light-weight paper at the conveyor

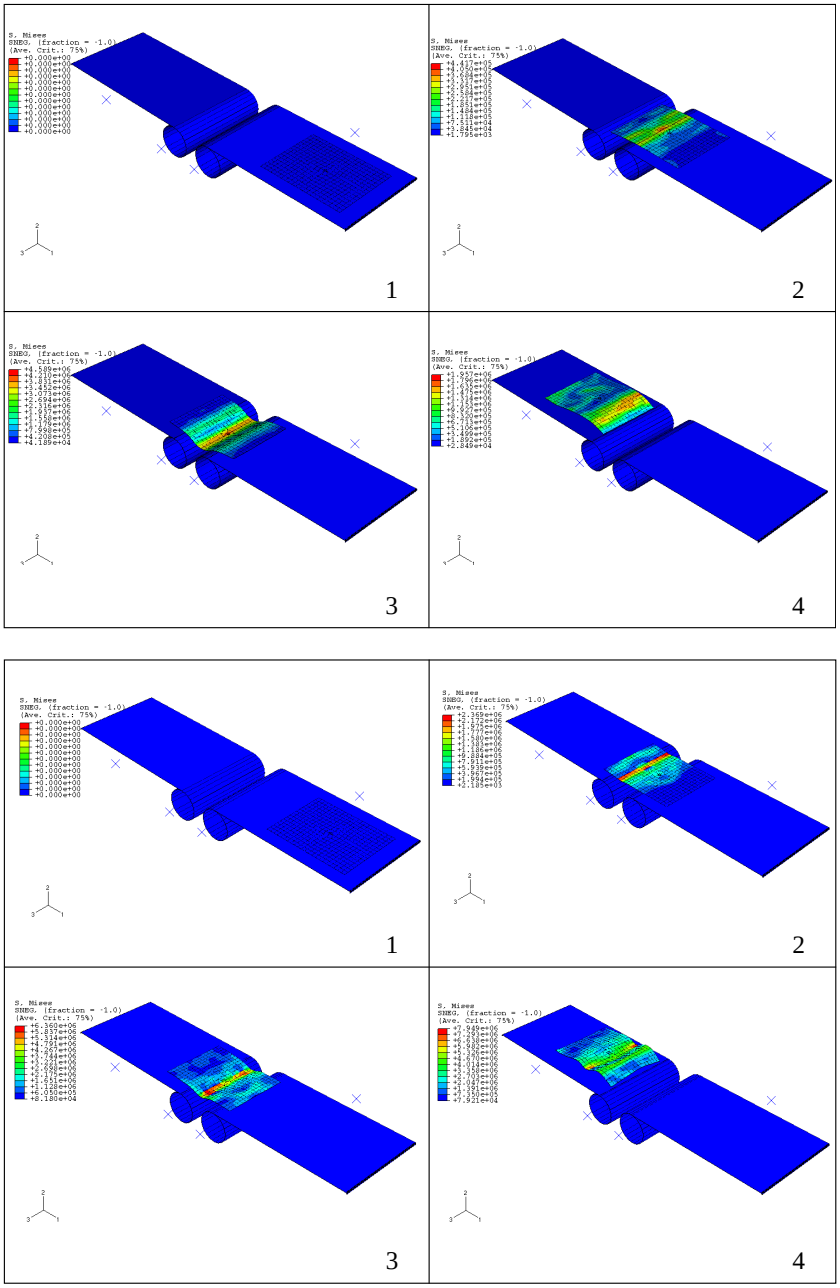

Figure 14. Response of heavy card stock when nozzle inlet pressure equals 20 psi. Top four panes: speed of 300 ft/min; bottom: 1200 ft/min.

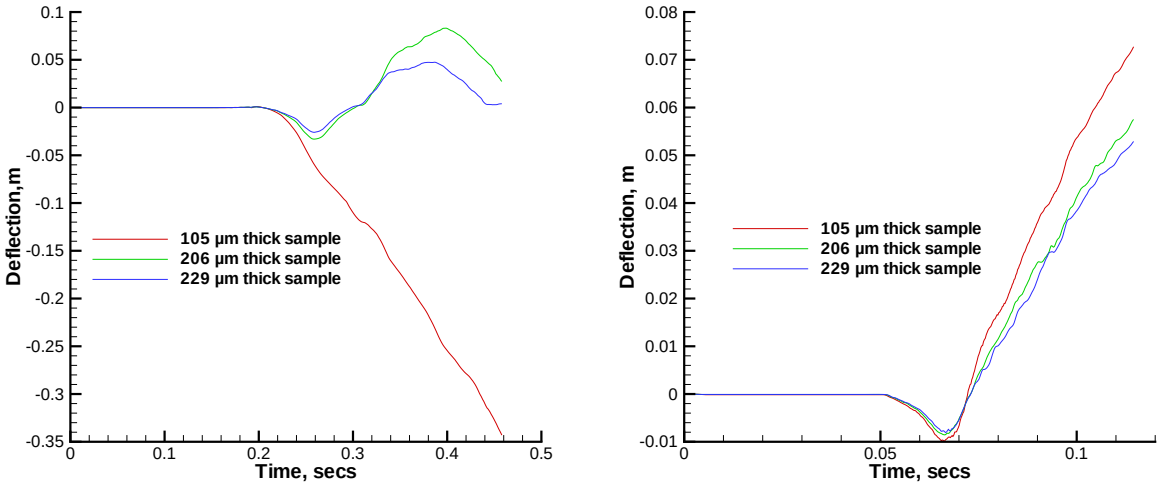

Figure 15. Time history of paper grades at a nozzle inlet pressure of 20 psi. Left: conveyor speed of 300 ft/min; right: 1200 ft/min.

speed of 1200 ft/min and at the nozzle inlet pressure of 20 psi. As expected there was an inverse relation between the bending stiffness and deflections of three samples; see Figure 16.

The thickness of the paper has the most influence in determining the bending stiffness of the paper. The basis weight is directly proportional to the thickness of the paper. Therefore the higher the basis weight, the lower the deflection. The basis weight of the sample is also related to the density of the sample. Paper such as heavy card stock, with higher value of density, when moving on high speed conveyor, will have more kinetic energy when compared to finer grades of paper. The kinetic energy of the sample influences the deflection and hence heavy card stock deflects less when compared to light-weight paper.

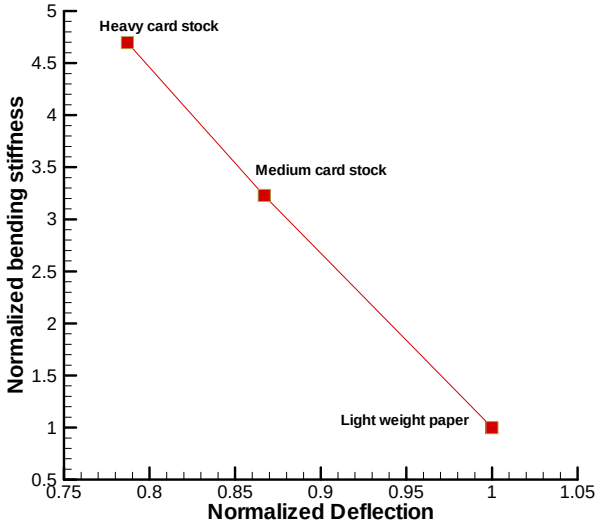

Figure 16. Variation of the sample deflection with respect to the bending stiffness.

4. Conclusions

A stiffness estimation method has been proposed for moving discrete paper samples on a high-speed conveyor. A finite element model of the sensing system, namely, the paper-conveyor system, with air impingement while the paper crosses over a gap, has been developed. The response of three dissimilar paper grades has been examined under different loading and boundary conditions. The influence of viscous pressure is shown to ensure that the sample will stick to the conveyor and successfully move with it and deflect under the influence of the impinging air jet. The deflection values estimated for the three grades at different speeds show that they could be ranked in terms of stiffness. Low stiffness samples, which fail to clear the gap at low conveyor speeds when the pneumatic load is applied, do clear the gap at high conveyor speeds. The orientation of the paper sample can be a confounding factor in decision making if the stiffness in MD and CD overlap between different grades, limiting the resolution that can be achieved in sorting. However, the method has sufficient resolution at operating speeds to distinguish between board and paper, which itself is a significant step in sorting mixed waste at high speeds.

References

[ABAQUS 2003] *ABAQUS analysis: user's manual*, Version 6.4, Hibbitt, Karlsson and Sorenson, Pawtucket, RI, 2003.

[Arzoumanian 2000] M. Arzoumanian, "Sorting the scientific way", *Official Board Markets* **76**:29 (2000).

[Brodeur et al. 1997] P. H. Brodeur, M. A. Johnson, Y. H. Berthelot, and J. P. Gerhardstein, "Noncontact laser generation and detection of Lamb waves in paper", *J. Pulp. Pap. Sci.* **23**:5 (1997), 238–243.

[Cheng and Berthelot 1996] J.-C. Cheng and Y. H. Berthelot, "Theory of laser-generated transient Lamb waves in orthotropic plates", *J. Phys. D Appl. Phys.* **29**:7 (1996), 1857–1867.

[Cornwell et al. 2001] M. Cornwell, Y. H. Berthelot, D. Griggs, and C. Habeger, "Noncontact determination of the bending stiffness of paper using laser ultrasonics and wavelet analysis: effects of moisture and temperature", pp. 747–750 in *IEEE Ultrasonics Symposium* (Atlanta, GA), vol. 1, edited by D. E. Yuhas and S. C. Schneider, IEEE, Piscataway, NJ, 2001. IEEE Catalog Number 01CH37263.

[Habeger et al. 1979] C. C. Habeger, R. W. Mann, and G. A. Baum, "Ultrasonic plate waves in paper", *Ultrasonics* **17**:2 (1979), 57–62.

[Hughes 1987] T. J. R. Hughes, *The finite element method: linear static and dynamic finite element analysis*, Prentice-Hall, Englewood Cliffs, NJ, 1987.

[Johnson 1996] M. A. Johnson, *Investigation of the mechanical properties of copy paper using laser generated and detected Lamb waves*, Ph.D. thesis, Georgia Institute of Technology, 1996.

[Leppänen et al. 2005] T. Leppänen, J. Sorvari, A. Erkkilä, and J. Hämäläinen, "Mathematical modelling of moisture induced out-of-plane deformation of a paper sheet", *Model. Simul. Mater. Sci. Eng.* **13**:6 (2005), 841–850.

[Makela and Ostlund 2003] P. Makela and S. Ostlund, "Orthotropic elastic-plastic material model for paper materials", *Int. J. Solids Struct.* **40**:21 (2003), 5599–5620.

[Mallapragada et al. 2004] V. Mallapragada, M. K. Ramasubramanian, and R. Venditti, "A compact, high speed lignin sensor for the automated sorting of newsprint from mixed waste", pp. 1137–1147 in *TAPPI Paper Summit: Spring Technical and International Environmental Conference* (Atlanta, GA), 2004.

[Mann et al. 1980] R. W. Mann, G. A. Baum, and C. C. Habeger, "Determination of all nine orthotropic constants for machine-made paper", *TAPPI J.* **63**:2 (1980), 163–166.

[Nilsson et al. 2001] C. M. Nilsson, L. Malmqvist, and J. Carlsson, "Red fluorescence sensor for noncontact on-line measurements in paper production", *Opt. Eng.* **40**:8 (2001), 1674–1681.

[Oden and Martins 1985] J. T. Oden and J. A. C. Martins, "Models and computational methods for dynamic friction phenomena", *Comput. Methods Appl. Mech. Eng.* **52**:1–3 (1985), 527–634.

[Pryor 2000] A. B. Pryor, "A paper sorting dream", *Scrap* **57**:5 (2000), 77–85.

[Ramasubramanian and Muthuraman 2003] M. K. Ramasubramanian and K. Muthuraman, "A computational mechanics model for the brim forming process in paperboard container manufacturing", *J. Manuf. Sci. Eng.* (*ASME*) **125**:3 (2003), 476–483.

[Ramasubramanian et al. 2005] M. K. Ramasubramanian, R. A. Venditti, C. Ammineni, and V. Mallapragada, "Optical sensor for non-contact measurement of lignin content in high speed moving paper surfaces", *IEEE Sens. J.* **5**:5 (2005), 1132–1139.

[Ridgway et al. 1999] P. Ridgway, A. Hunt, M. Quinby-Hunt, and R. Russo, "Laser ultrasonics on moving paper", *Ultrasonics* **37**:6 (1999), 395–403.

[Ridgway et al. 2003] P. Ridgway, R. Russo, E. Lafond, C. Habeger, and T. Jackson, "Laser ultrasonic system for on-line measurement of elastic properties of paper", *J. Pulp Pap. Sci.* **29**:9 (2003), 289–293.

[Roman and Jeffers 1992] G. Roman and L. Jeffers, "Development of a prototype lignin concentration sensor", pp. 44 in *DOE/Industry Advanced Sensors Technical Conference*, 1992.

[Seo et al. 1992] Y. B. Seo, B. Castagnede, and R. E. Mark, "An optimization approach for the determination of in-plane elastic constants of paper", *TAPPI J.* **75**:11 (1992), 209–214.

[Singhal et al. 2001] D. K. Singhal, C. Dushyant, and J. Singh, "Fuzzy logic and sorting of waste paper", *IPPTA J.* **13**:1 (2001), 25–27.

[Sun et al. 2000] J. S. Sun, K. H. Lee, and H. P. Lee, "Comparison of implicit and explicit finite element methods for dynamic problems", *J. Mater. Process. Technol.* **105**:1–2 (2000), 110–118.

[Walter et al. 2000] J. B. Walter, T. L., J. P. Gerhardstein, B. M. Pufahl, C. C. Habeger, M. Lafonde, and P. H. Brodeur, "Fabry–Perot laser ultrasonic elastic anisotropy measurements on a moving paper web", pp. 247–254 in *Review of progress in quantitative nondestructive evaluation: proceedings of the 26th annual Symposium on Qualitative Nondestructive Evaluation* (Montréal, 1999), vol. 19A, edited by S. Kallsen et al., AIP Conference Proceedings **509**, AIP, Melville, NY, 2000.

[Zhong 1993] Z. H. Zhong, *Finite element procedures for contact-impact problems*, Oxford University Press, New York, 1993.

Received 6 Jun 2006. Accepted 28 Aug 2006.

M. K. RAMASUBRAMANIAN: rammk@ncsu.edu
Department of Mechanical and Aerospace Engineering, 1217 Broughton Hall, Campus Box 7910, North Carolina State University, Raleigh, NC 27695-7910, United States
http://www.mae.ncsu.edu/homepages/ram/index.html

RICHARD A. VENDITTI: richard_venditti@ncsu.edu
Department of Wood and Paper Science, North Carolina State University, Raleigh, NC 27695-7910, United States
http://www4.ncsu.edu/unity/users/r/richardv/www

KALYAN C. KATURI: kckaturi@ncsu.edu
Department of Mechanical and Aerospace Engineering, North Carolina State University, Raleigh, NC 27695-7910, United States